Production of bacterial cellulose nanocrystals via enzymatic hydrolysis and evaluation of their coating on alginate particles formed by ionotropic gelation

Victória S. Soeiro [a], Louise L. Tundisi [b], Letícia C.L. Novaes [b], Priscila G. Mazzola [b], Norberto Aranha [a], Denise Grotto [c], José M.O. Júnior [d], Daniel Komatsu [e], Francisco M.P. Gama [f], Marco V. Chaud [g], Angela F. Jozala [a,*]

[a] LAMINFE – Laboratory of Industrial Microbiology and Fermentation Process, University of Sorocaba, Sorocaba 18023-000, Brazil
[b] Faculty of Pharmaceutical Sciences, State University of Campinas, Campinas 13083-871, Brazil
[c] Lapetox – Laboratory of Toxicology Research, University of Sorocaba, Sorocaba 18023-000, Brazil
[d] LAFINAU – Laboratory of Nuclear Physics, University of Sorocaba, Sorocaba 18023-000, Brazil
[e] Laboratory of Biomaterials, Pontificial University Catholic, Sorocaba, SP, Brazil
[f] CEB – Centre of Biological Engineering, University of Minho, Braga 4710-057, Portugal
[g] LABNUS – Biomaterials and Nanotechnology Laboratory, University of Sorocaba, Sorocaba 18078-005, Brazil

ARTICLE INFO

ABSTRACT

This study aimed to obtain the bacterial cellulose nanocrystals (CNC) by enzymatic hydrolysis and verify the CNC application as coating material in alginate particles. Therefore, the production of CNC was carried out through two enzymatic hydrolysis methods involving a time period of 48 and 72 h. 0.35 mg of dry mass of cellulose was produced approximately 1.6×10^{11} CNC/mL. The CNC obtained by enzymatic hydrolysis at 72 h (Method II) was applied to cover the alginate particles, obtained by ionotropic gelation. The CNC Zeta potential value was about $+15$ mV and for alginate particles -26.46 ± 1.48 mV. These results confirmed the application of CNC as coating material for alginate particles. It brings an incremental contribution to the knowledge advancement in the pharmaceutical and food area, allowing the engineering of systems to use a mixed composition of nano-biomaterials to modify the release pattern of drugs, macromolecule, nutrients, stabilizers and target specific drug release.

1. Introduction

Bacterial cellulose (BC) is a biopolymer produced by bacteria and has the same molecular structure as plant cellulose. However, BC is free from lignin, pectin, and hemicelluloses. In addition, BC has many advantages such as higher degree of polymerization, higher crystallinity, higher mechanical properties than plant cellulose. These characteristics make BC a better option for several applications (Dugan, Gough & Eichhorn, 2013; Vasconcelos et al., 2017). One of the BC applications is changing the structures from macro to nano level to obtain rigid rod-shaped particles and cellulose nanocrystals (CNC) (Abol-Fotouh et al., 2020; Habibi, Lucia & Rojas, 2010; Qiu & Netravali, 2014).

CNC is a low-cost material with good biocompatibility and biodegradability, renewable and sustainable, being derived from bacterial cellulose. It has completely stretched chain segments with an almost perfect crystalline structure, with mechanical resistance, large surface area, low toxicity and several applications (George & Sabapathi, 2015; Yan et al., 2018) in food industry (George et al., 2014), nanotechnology (Pirich, de Freitas, Torresi, Picheth & Sierakowski, 2017), and the pharmaceutical industry (Yan et al., 2018).

To produce CNC, there are different methodologies including chemical, enzymatic or mechanical treatments (Dugan et al., 2013). The enzymatic process consists of applying enzymes capable of degrading cellulose. The production of CNC by enzymatic process is considered eco-friendly as it does not generate acid residues, however is a challenging (Alonso-Lerma et al., 2020; Choi & Shin, 2020). Also, by using enzymes, it is possible to maintain the native properties of cellulose, such as structure and thermal stability, making it an alternative for

obtaining nanocrystals (George, Ramana & Bawa, 2011; Rovera et al., 2018).

For pharmaceutical applications, this work was based on the interactions of CNC with anionic materials to develop drug delivery system (You et al., 2016). Emulsions are immiscible liquid systems stabilized by surfactants, forming two (oil/water or water/oil) or multiple (water/oil/water or oil/water/oil) phase systems (Morais et al., 2018; Sousa et al., 2017). The advantage of emulsion systems are simultaneously solubilizing hydrophilic and fat-soluble drugs, controlling the release of the drug, increasing the permeation of drugs, masking taste and odor, and improving the palatability of the final product (Kale & Deore, 2017).

Herein, we have demonstrated how to apply an alternative way to produce matrix by ionotropic gelation utilizing alginate. Ionotropic gelation is a process where interaction occurs between polymer and oppositely charged other agent. This technique uses polymers of natural origins to produce biocompatible and biodegradable biomaterials. In addition, it has the ability to incorporate fat-soluble agents (Benavides, Cortés, Parada & Franco, 2016; Patel, AbouGhaly, Schryer-Praga & Chadwick, 2017).

Alginate is a polymer extracted from natural sources, which is widely used in the area of pharmaceutics and tissue engineering. This material has several advantages, including the facilitation of blood clotting, activation of the immune system, bactericidal effect, among others (Ng, Migotto, Ferreira & Lopes, 2017; Yan et al., 2018). Castor oil is a viscous, pale-yellow, non-volatile, non-drying material extracted from castor seeds (*Ricinus communis*). This product is cost effective, has long self-life and prevents the formation of peroxide (Patel, Dumancas, Viswanath, Maples & Subong, 2016).

The utilization of bacterial cellulose with alginate composites has already been reported. However, (Kim et al., 2017) the researchers ran the tests with whole membrane (not hydrolysed). And in other studies, the researchers ran the tests with CNC derived from plants to coat the alginate (Criado et al., 2019; Ma et al., 2019; Mohammed, Grishkewich, Berry & Tam, 2015). In this work, the novelty was alginate particles covered with CNC derived from bacterial cellulose.

Although there is widespread literature about cellulose nanocrystals production, but there are few reports on bacterial nanocellulose and enzymatic processes to produce CNC. For this reason, we have studied the influence of different parameters for nanocrystals production and its possibilities in pharmaceutical applications. With this background, the aim of this work was to obtain nanocrystals by enzymatic hydrolysis and develop alginate particles, by ionotropic gelation, to coat the particles with CNC.

2. Materials and methods

2.1. Bacterial nanocellulose production

Bacterial cellulose was produced by *Komagataeibacter xylinus* (ATCC 53,582), in Hestrin & Schramm broth (20 g/L glucose, 5 g/L bacteriological peptone, 5 g/L yeast extract, 2.7 g/L sodium phosphate anhydrous; 1.5 g/L citric acid monohydrate). Bacteria were grown in 125 mL Erlenmeyer flasks with a 50 mL of HS broth inoculated with around 10^6 CFU/mL (Jozala et al., 2014). The flasks were incubated at 30°C for 15 days in static condition. After 15 days, the BC membranes were collected, washed and put through a bleaching stage, with a 1 M sodium hydroxide solution for 1.5 h at 60 °C and rinsed until reaching pH 7.0. The membranes were stored in flasks with ultrapure water and subsequently sterilized at 121 °C for 15 min.

2.2. Production of CNC

In a pilot test (Appendix A), the enzyme concentration, the bacterial cellulose amounts and the time of hydrolyses for the production of CNC were pre evaluated. The best condition for the CNC production by enzymatic hydrolysis was observed in 48 h, with 100 μL/mL of enzyme per 0.1 g of bacterial cellulose.

2.2.1. Method I: 5-step production

In the first step, the mechanical process was performed with the ultra-turrax (IKA T25 digital) (12,500 rpm for 5 min - 3 times). The bacterial cellulose suspension was centrifuged at 5500 rpm for 20 min and the precipitated, cellulose mass, was removed for enzymatic hydrolysis.

In the second step, the enzymatic process, 0.35 g of the cellulose mass, with 99% humidity determined by a humidity scale, was placed in a 15 mL Falcon tube with 1 mL of acetate buffer solution (0,1 M, pH 5) and 150 μL of cellulase (Sigma Aldrich, cellulase from *Trichoderma reesei*, aqueous solution, ≥ 700 units/g) . The tubes were incubated in an orbital shaker at 150 rpm at 50 °C for 48 and 72 h.

In the third step, the samples were placed in a thermostatic bath at 80°C for 20 min for enzymatic inactivation. After 20 min, 1 ml of ultra-purified water was added.

In the fourth step, the separation process was based on three centrifugations at 5500 rpm for 20 min. The sample supernatants were removed every 20 min, and 2 ml of ultra-purified water was added and vortexed for 1 min. In the second centrifugation, the supernatants were collected and identified as C samples; and in the third centrifugation, the supernatants were collected and identified as E samples.

In the fifth step, the purification process, samples C and E were kept in an ultrasonic bath at 35°C for 20 min. Then, the samples were filtered through a 450 nm PTFE filter and stored in 2 ml Eppendorf tubes at 8 °C for 21 days.

2.2.2. Methodology II: production by high-pressure homogenizer and filtration

The second methodology was performed based on the results of the first methodology. Two unit operations of the prior process were modified. In the first step, the sample was submitted to the high-pressure homogenizer (Homo lab 2.20 FBF Italia) at 1400 bars, in two cycles. And in the fifth step, the 450 nm filter was replaced by a 220 nm filter. These adjustments were made to decrease the size and agglomeration of the CNC, improving their stability.

2.3. Glucose release from cellulose biomass conversion by enzymatic hydrolysis

The enzyme concentration and hydrolysis time were determined based on other studies carried out by our research group (supplementary material). In this present work, the enzymatic action in CNC's production was analyzed by the glucose released in the medium and the pH change of the process. Glucose was determined by Sigma Glucose (GO) Assay Kit and cellulose conversion by the Eq. (1):

$$\frac{Abs\,540\,nm_{sample\_test} \times Glucose\,in\,standard\,sample_{mg}}{Abs\,540\,nm_{standard}} \quad (1)$$

The released sugars in the hydrolysate were quantified and it was possible to observe the bacterial cellulose conversion yield by the Eq. (2).

$$\%C = \frac{C\,glu \times 0,9 \times V}{C\,mass} \times 100 \quad (2)$$

where %C is the cellulose conversion yield, C_{glu} is the glucose concentration (mg/mL), C_{mass} is the real mass of the cellulose in material, 0.90 is the cellulose-to-glucose conversion factor, and v is the reaction volume (adapted from Pereira and Arantes 2020).

2.4. Characterization of CNC

The characterization was performed to evaluate the size,

Table 1
Formulation of emulsified system.

	Reagent	Quantity (g)
Oil phase	Hydroxylated and ethoxylated castor oil (OR-HE) EHL13	35
Water phase	Sodium alginate medium viscosity	3.75
	Mixture of surfactant * EHL 12.86	2.5
	Ultra purified water	209

*Tween 80 EHL 15 (80%) and Span 80 EHL 4.3 (20%).

polydispersity by the dynamic light scattering (DLS) technique; and zeta potential (BrookHaven - NanoBrook plus), at an angle of 90° at 25 °C. The observations were made at 0, 4, 7, and 21 days in order to analyze its stability, as the CNC may vary in size, degradation, or agglomerate over time. In these analyses, the samples were diluted 1:10 with purified water in triplicate to avoid multi-scattering phenomena. The results were demonstrated in nanometers (nm) for alginate particle diameter and in millivolts (mV) for zeta potential (de Souza et al., 2020).

The samples with the best results were selected and characterized by Nanoparticle tracking analysis (NTA), which determines the refractive index of suspended nanoparticles. The method is based on the Brownian movement, being able to evaluate the size and concentration of nanoparticles in the sample (Juárez-luna, Favela-torres, Quevedo & Batina, 2019; Niskanen et al., 2019). The measurements were carried out using 1 mL of diluted samples at a ratio of 1:100.

For SEM procedure, the sample was diluted at a ratio of 1:100, added on top of a carbon strip, dried at 50 °C for 2 h, and analysed on the FEI Quanta 650 FEG equipment. For the TEM analysis, the sample was diluted at a ratio of 2:10. The sample was homogenized in a vortex, ultrasonication and 3 to 5 drops of the sample were placed on a carbon grid with a filter paper.

2.5. Preparation of the emulsified system

The emulsion of castor oil, sodium alginate and water was obtained by mixing an aqueous phase and a modified oil phase (Deepak & Hari, 2013). Table 1 shows the formulation of the emulsified system.

The castor oil (OR-HE) was heated to decrease the viscosity ($\sim$ 60 °C), while the aqueous phase was heated to a slightly higher temperature ($\sim$ 65°C). The two phases were mixed under constant and vigorous stirring, and then the dispersion was cooled to 25 °C. The emulsion obtained was homogenized under pressure, 600 bar (60×10^3 kPa) for two cycles (Homo lab 2.20 FBF Italia).

2.6. Obtaining alginate particles by ionotropic gelation

Ionotropic gelation technology was applied to obtain the alginate particles. The emulsified system was added drop by drop with a 26 G needle into a 2 M calcium chloride solution, under constant agitation, with a peristaltic pump kept at a constant speed for 1 h.

2.7. Alginate particles coated with CNC

The alginate particles were washed with ultra-purified water in order to remove the excess calcium. After washing, 4 g of the particles were immersed in 50 ml of pH 8.5 potassium phosphate buffer solution and kept in an orbital shaker at 100 rpm for 1 h at 25 °C.

After this period, 2 g of the alginate particles were collected and put in a solution with 1.6×10^{11} CNC/mL, in an orbital shaker at 100 rpm at 25 °C for 48 h, while the other 2 g were kept in ultrapure water as a reference sample.

2.8. Alginate Particle morphological and physical-chemical characterization

The alginate particles were characterized by the techniques of zeta potential, differential scanning calorimetry (DSC), Fourier-transform
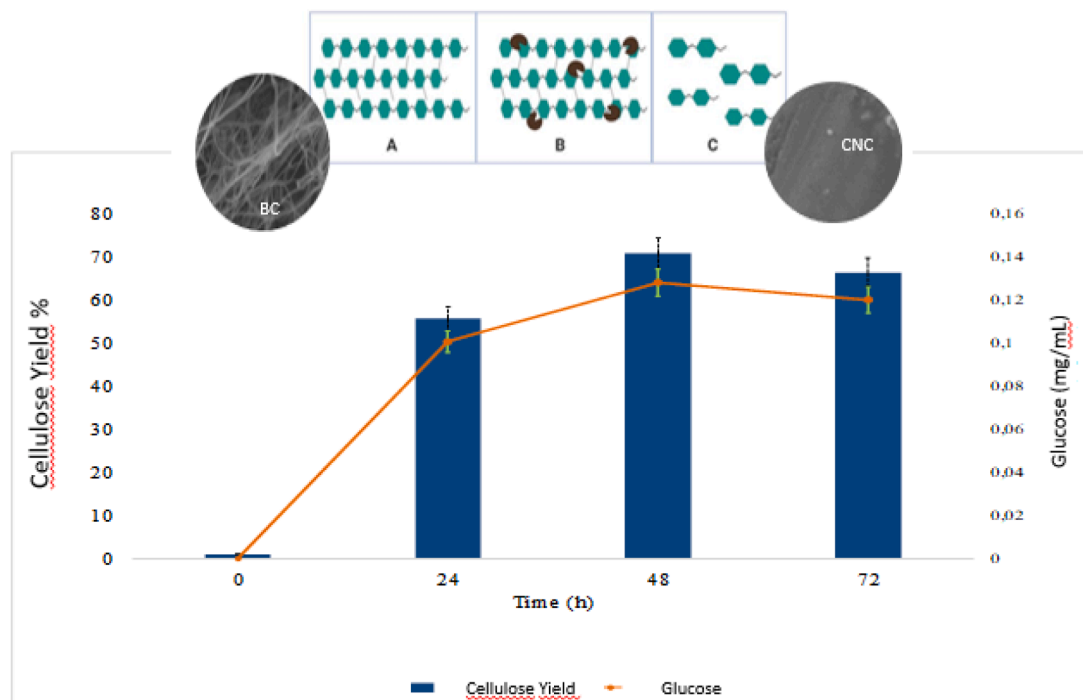

Fig. 1. Glucose release after enzyme interaction and cellulose amount converted during the reaction, at different intervals: 0, 24, 48, and 72 h, at pH 5.0. The Scheme of enzyme reaction is exemplify in (A) Bacterial cellulose glucose units connected through β-1,4-glycosidic bonds; (B) Enzyme [black circles] hydrolyzing β-1,4-glycosidic bonds in the cellulose fibers; (C) Bacterial cellulose nanocrystals and molecule glucose being released. The left microscopic shows the bacterial cellulose before the enzymatic reaction and the right image shows after the enzymatic reaction.
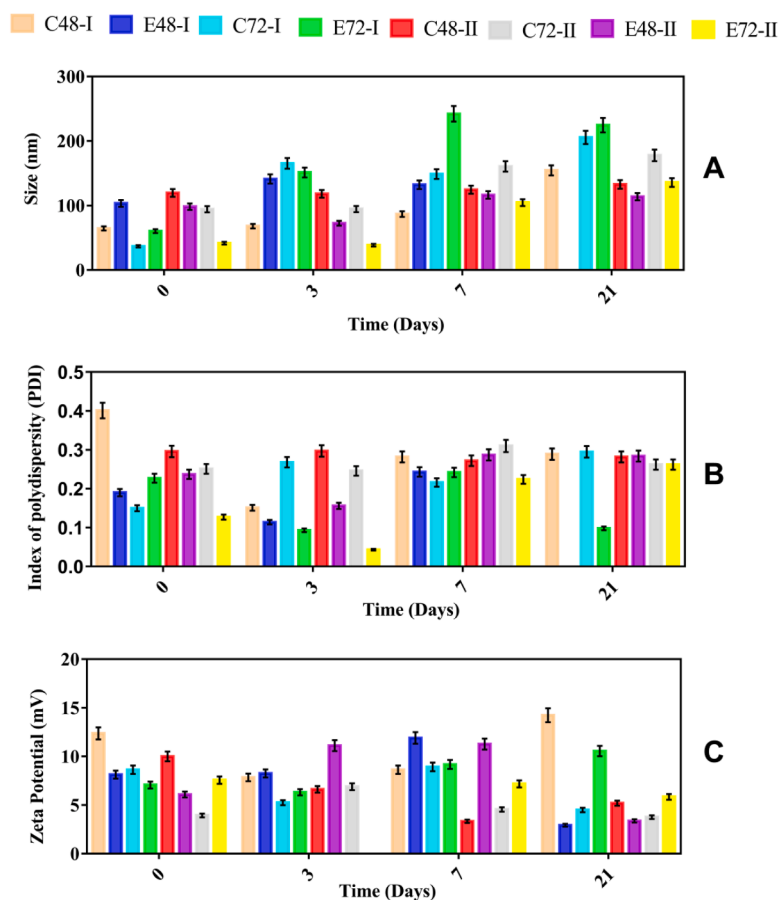
Fig. 2. Size (A), index of polydispersity (B) and potential zeta (C) characterization of CNC samples produced by different processes and evaluated in the period of 0, 3, 7, and 21 days. Sample C - two times centrifugated Sample E – three times centrifugated; Sample 48 - 48 h of hydrolysis, Sample 72 - 72 h of hydrolysis; Sample I - ultra-turrax and 450 nm filtration; Sample II – high-pressure homogenizer and 220 nm filtration.

infrared spectrometry (FTIR), optical microscopy, and scanning electron microscopy (SEM) (Alves et al., 2018).

The zeta potential of the alginate particles in the absence of CNC was measured by the SurPASS 3 (Anton paar). The analysis was performed in duplicate, under pressure between 200 and 600 bars at pH values ranging from 4.5 to 9.

The DSC characterization was performed by the Thermal Analyzer (Shimadzu TA-60, Kyoto, Japan). A 2 mg sample was packed in an aluminum pan and heated under nitrogen with a flow of 50 mL/min from 25 to 400 °C. For the CNC, liquid sample, a heating rate of 2°C/min was used whereas for the reference alginate particles and particles covered with CNC, solid samples, it was 10°C/min.

The CNC, reference alginate particles, and alginate particles with CNC samples were analyzed by FT-IR (Shimadzu, IRAffinity-1, Kyoto, Japan) via Labsolutions Software v.2.10. The samples were prepared on KBr disks by a hydraulic press. The infrared spectra were recorded in the range of 400–4000 cm^{-1} with a resolution of 4 cm^{-1} and 32 scans.

The alginate particles were observed under an optical microscope to check for changes in the morphology of the reference alginate particles and alginate particles with CNC. The images were taken at intervals of 0, 6, 10, 24, and 48 h, observing the difference between them.

For SEM, the alginate particles were placed in a 1% sucrose solution, stored at -80 °C for 24 h, and lyophilized for 72 h. The samples were fixed with carbon tape, subjected to metallization for 2 min (DH-29010SCTR Smart Coater), and analyzed on the scanning electron microscopy equipment (JSMIT200).

2.9. Statistical analysis

Differences among samples were presented as mean ± standard deviation. *P* values <0.05 were considered significant. Data were analyzed using Statistica®8.0 (Statsoft software, Tulsa, OK, USA).

3. Results and discussion

3.1. CNC production

3.1.1. CNC glucose release and conversion yield

Fig. 1 shows the amount of glucose released after the bacterial nanocellulose was submitted to the enzymatic hydrolysis process, and the amount of cellulose converted in the reaction.

In Fig. 1, it is possible to observe that the glucose concentration increased 5 times, reaching 0.10 mg/mL, pH 5, from 0 to 24 h; and after 48 h, there was a slight increase, reaching 0.12 mg/mL, pH 5, which remained constant until 72 h. The highest coverstion was around 70% in 48 h.

When CNC glucose release was available, similar results were observed in Kafle, Shin, Lee, Park and Kim (2015) that analyzed the bacterial cellulose enzymatic hydrolysis in order to understand the structural changes in different periods of time (12, 24, 48, 72 and 96 h), utilizing 5% (w/v) of the sample and enzyme. They observed the highest conversion rate during the first 12 h, around 50%, reaching approximately 70% in 72 h.

3.1.2. CNC size characterization

The average size, index of polydispersity and potential zeta of CNC

Table 2

NTA analysis of CNC samples.

Sample	Size NTA (nm)	Size DLS (nm)	Concentration (nanoparticles/mL)
C72 – II	246 ± 9.2	94,3 ± 21,22	$1,66 \times 10^{11} \pm 3,72 \times 10^{9}$
E72 – II	242.8 ± 4.3	41,67 ± 5.55	$1,57 \times 10^{11} \pm 4,47 \times 10^{9}$

Sample C - two centrifuges; Sample E - three centrifugations; Sample 72 - 72 h of hydrolysis. Sample I - ultra-turrax and 450 nm filtration; Sample II - high pressure homogenizer and 220 nm filtration.

throughout 21 days is reported in Fig. 2.

The size of the CNC (2.A) varied between 37 and 242 nm in 21 days, with all samples showing an increase in the size of 4.1 to 303% from the third day. The CNC samples that were hydrolyzed for 48 h showed and maintained the size between 65 -155 nm along the 21 days. The 72 h samples showed values between 37 - 242 nm. In the 72 h sample, there was a decrease in the size of the CNC. However, lower values were observed in the samples treated in the 48 h period, indicating that the time of enzymatic hydrolysis has a direct impact on CNC size.

When evaluating the number of centrifugations to obtain the CNC (two - C or three - E) throughout the test, it was not possible to identify changes in the size of the CNC, with the size varying from 37 to 205 nm for C and 39 to 225 nm for E. Thus, centrifugation was not a parameter that affected the production of CNC.

According to George et al. (2011), the CNC produced by enzymatic hydrolysis has sizes between 100–300 nm. Kafle et al. (2015) observed that the time of enzymatic hydrolysis is directly linked to the size of the CNC. Therefore, reaction time is an important parameter in the methodology for obtaining CNC.

Therefore, when combining mechanical treatment, filtration, and three centrifugations, it was possible to obtain smaller CNC sizes. As we can observe in methodologies I and II. In methodology I (without homogenizer and filtration), CNC was obtained between 36.9 ± 1.35 and 224.57 ± 10.49 nm. When adding unit operations (methodology II), the values ranged from 38.67 ± 1.73 and 177.8 ± 15.25 nm, influencing the size of the CNC.

Chauve, Fraschini and Jean (2014) reviewed about centrifugation and filtration steps to remove agglomerates in the final CNC sample. However, its application is restricted to acid hydrolysis and CNC of plant origin. In our studies, it was possible to observe that unit operations were also fundamental to obtain smaller and more stable CNC from
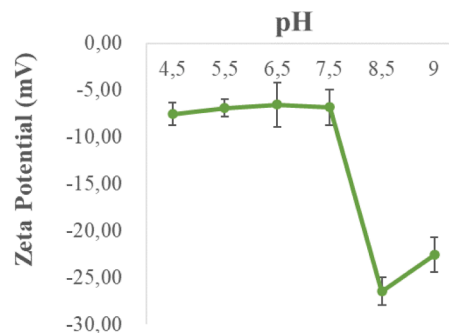

Fig. 4. Result of the zeta potential of alginate particles without CNC.
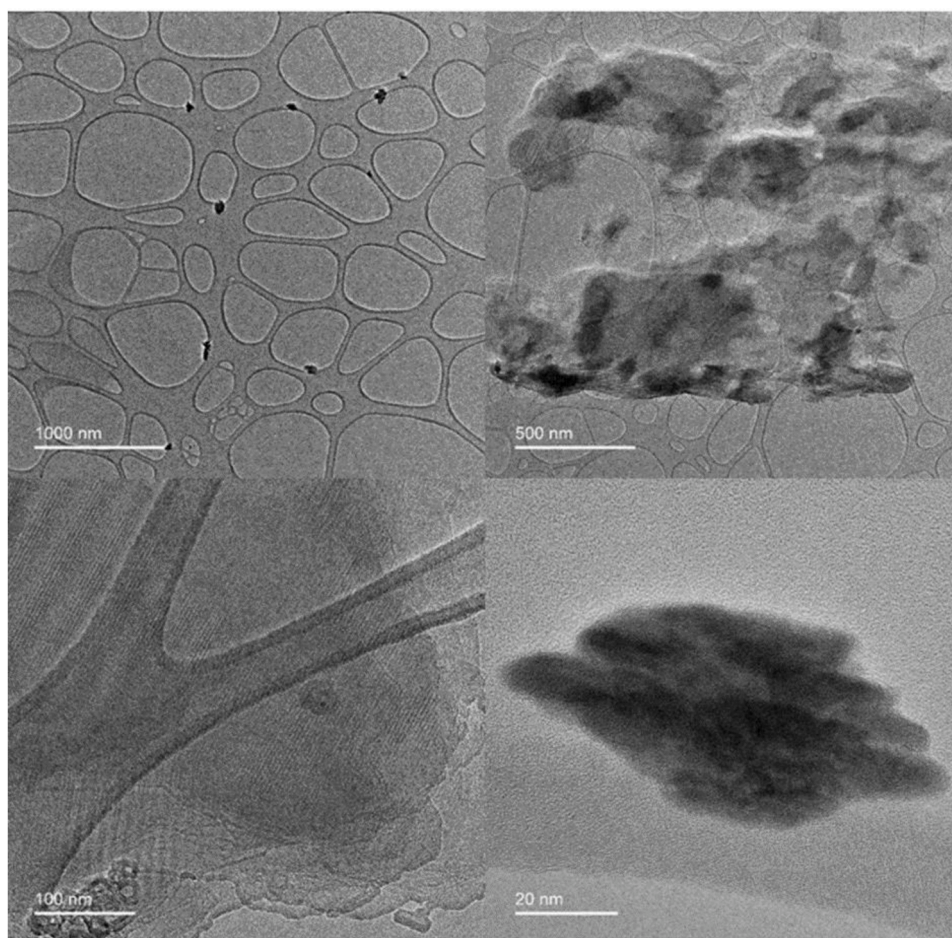

Fig. 3. Transmission electron microscopy (TEM) of the sample of bacterial cellulose nanocrystals (CNC). Bacterial cellulose (CNC) nanocrystals in 1000, 500, 100, and 20 nm scale.
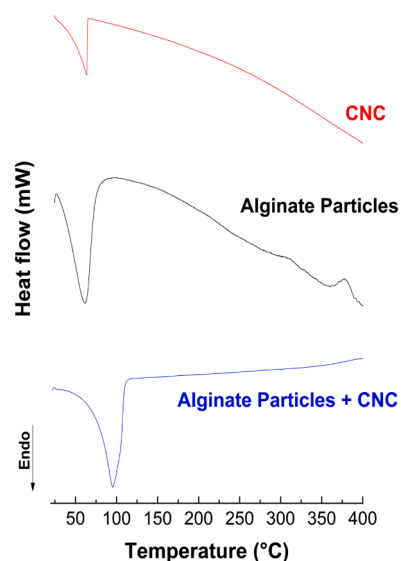
Fig. 5. Results of DSC analysis containing the thermogram of the alginate particles, alginate particles + CNC, and CNC samples. CNC - Bacterial cellulose nanocrystals.

bacteria.

George et al. (2011) studied the CNC production using the same enzyme (cellulase from *Trichoderma reesei*, aqueous solution, ≥700 units/g, Sigma Aldrich). However, the greatest advantage was the ratio of cellulose/acetate buffer/enzyme. While they mixed 0.1 g cellulose in 1 mL of the acetate buffer + 1 mL of cellulase, in our study, we mixed 0.35 g cellulose in 1 mL of the acetate buffer + 0.15 mL of cellulase. In our work, we applied 6,66 times less enzyme and the hydrolysis was 3.5 times more efficient than in their study. Moreover, they did not apply filtration process in their samples.

Rovera et al. (2018) studied the enzymatic hydrolysis of BC to obtain nanocrystals applying ultra-turrax, followed by freeze-drying. For the hydrolysis process, they used cellulase enzyme. In a more recent paper of Rovera, Fiori, Trabattoni, Romano and Farris (2020), the hydrolysis of BC was run using two different enzymes - endo-1,4- -glucanase and cellulase. The methodology is similar to the paper from 2018, but they ran the hydrolysis process to select the amorphous regions. In both

studies, Rovera and colleagues did not run the filtration process. In comparison to our methodology, we used only one type of enzyme, making the process less expensive and, also managing filtration, which improves the particles separation. In addition, we were able to decrease the size of the nanoparticles by about 4 times.

Fig. 2.B shows the results of the polydispersity index (PDI) test of CNC samples. We can observe that the data varied between 0.043 ± 0.026 and 0.401 ± 0.024 along the 21 days of testing, with all samples showing a more stable value from day 7.

Regarding the hydrolysis time, the PDI values of 48 h were greater than those in the samples of 72 h. The values varied throughout the experiment between 0.114 ± 0.083 and 0.401 ± 0.024 for 42 h; 0.043 ± 0.026 and 0.295 ± 0.043 for 72 h. Therefore, by increasing the hydrolysis time, it is possible to obtain a lower polydispersity index of the samples.

The number of centrifugations factor (C - two and E - three) was a relevant parameter for the PDI values. The variation of the PDI along the 21 days for samples C was 0.15 ± 0.039 and 0.401 ± 0.024, and for samples E, it was 0.043 ± 0.026 and 0.287 ± 0.019. This represents the formation of uniform CNC populations when using three centrifugations in the methodology.

Samples performed without homogenization and filtration (methodology I) showed values between 0.114 ± 0.083 and 0.401 ± 0.024 throughout the test. The values of the samples with the addition of the unit operations (methodology II) were between 0.043 ± 0.026 and 0.297 ± 0.017. Therefore, methodology II demonstrated lower values of PDI, variation between data, and standard deviation of the samples.

The PDI demonstrates the degree of uniformity of the samples. Some studies used filtration, centrifugation, or ultracentrifugation to decrease the heterogeneity of CNC and concluded that these unit operations can make samples more uniform and with a lower polydispersity index, as in our work (Bai, Holbery & Li, 2009; Chauve et al., 2014; Danaei et al., 2018; Elazzouzi-hafraoui et al., 2008).

Yan et al. (2017) analyzed the PDI before and after hydrolysis of bacterial cellulose and the value changed from 0.41 to 0.25. Although the methodology used in the study was acid hydrolysis, it confirms the importance of performing the hydrolysis step to decrease the PDI values.

The CNC is considered stable when the absolute value is higher than 25 mV or lower than− 40 mV when hydrolysed by acids (J. P. S. Morais et al., 2013; Morantes, Muñoz, Kam & Shoseyov, 2019). In the Fig. 2.C, shows the results along the 21 days, the 48 h samples showed values between 2.93 ± 0.85 mV and 14.24 ± 4.52 mV. For the 72 h samples, the
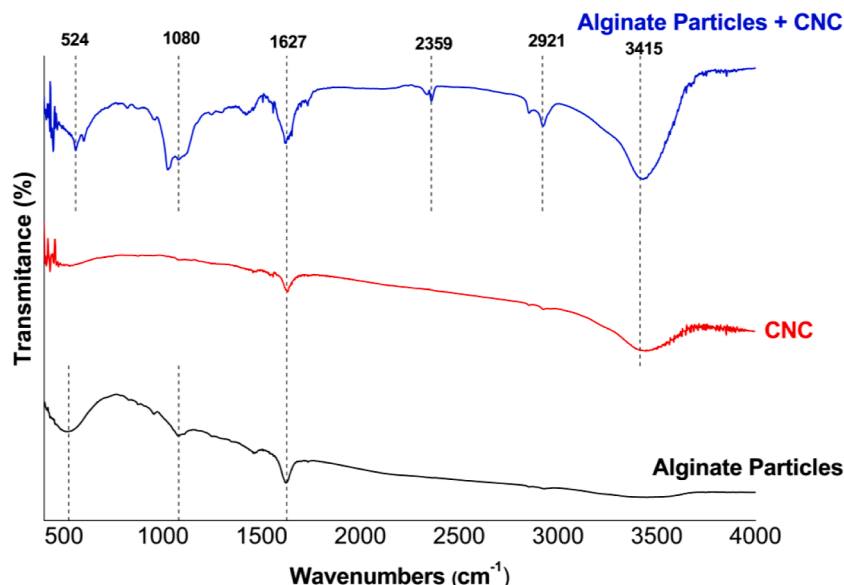

Fig. 6. FTIR analysis result containing spectra of reference alginate particles, alginate particles + CNC, and CNC samples. CNC – Bacterial Cellulose Nanocrystals.
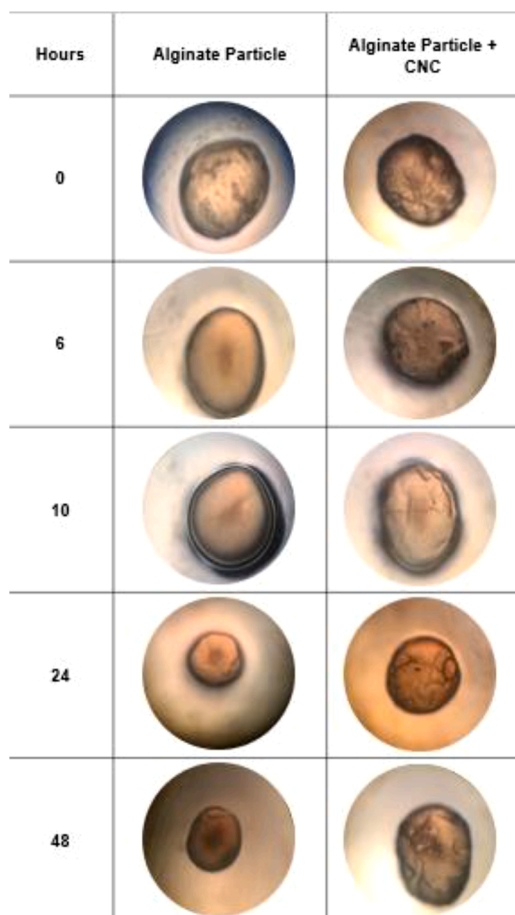
Fig. 7. Optical microscopy at 40x magnification of alginate particles and alginate particles coated with CNC in different time 0, 6, 10, 24, and 48 h. CNC – Bacterial cellulose nanocrystals. Scale bars image of 0.1 mm.

values were 3.76 ± 1.68 mV and 10.56 ± 3.17 mV. Even though, In the Fig. 2.C, shows the results of the zeta potential lower than 25 mV, a fundamental point to be highlighted is the CNC in this work was hydrolysed by enzyme. Thus, the resultant CNC could form a stable aqueous suspension when was immediately applied. As have shown here, when CNC was contact with alginate particles.

The results regarding the number of centrifugations did not show any significant difference during the test period either. For two centrifugations (sample C), the values ranged between 3.335 ± 0.44 mV and 14.24 ± 4.52 mV, whereas for three centrifugations (sample E), the data ranged between 2.93 ± 0.85 mV and 11.91 ± 1.69 mV.

Methodology I (without homogenizer and filtration) had values between 2.93 ± 0.85 mV and 14.24 ± 4.52 mV along the 21 days. For methodology II with unit operations, the data were between 3.37 ± 1.27 mV and 11.28 ± 0.1 mV. These results indicate that the variation of unit operations did not affect the evaluated parameter.

One of the major problems faced when producing CNC by enzymatic hydrolysis is post-hydrolysis re-aggregation, which occurs due to random erosion of the crystalline surface of the particles (Rovera et al., 2018). The suggestion of Rovera and collaborators is the utilization of surfactants or polyelectrolytes to modify the surface of CNC. However, it is known that some surfactants, such as anionic and cationic ones, induce adverse effects (irritation and hemolysis), and their by-products cause environmental problems (Wang, Law, Chen, Chen & Tang, 2017; Yi et al., 2017). In our study, the solution was applied immediately the CNC to cover alginate particles.

The widespread use of acid hydrolysis is due to its ease of obtaining more stable CNC. The acid acts on the surface of the CNC,

electrostatically stabilizing them with negative charges, without changing the surface of the nanomaterial and forming a homogeneous dispersion in an aqueous medium (Arserim-uçar, Korel, Liu & Yam, 2020). However, by using enzymatic hydrolysis in the process, a more ecological product is obtained without generating waste to the environment (George et al., 2011).

3.1.5. Nanoparticles tracking analysis (NTA)

The samples with the best results of size, PDI and zeta, were chosen for the NTA assays (Table 2), with samples C72-II (second centrifugation, 72 h of hydrolysis, methodology II) and E72 - II (third centrifugation, 72 h of hydrolysis, methodology II).

It is evident from Table 2 there was no statistical difference between the samples, so the concentration of the nanoparticles does not depend on unit operations (methodologies I and II). In the two samples, the initial dry cellulose mass was 0.35 mg/mL, which generated approximately 1.6×10^{11} CNC/mL. When comparing the size values by the techniques of NTA and DLS, it is possible to observe a great difference between them.

Rovera et al. (2018) calculated the yield of CNC through spectrophotometer and by weight of the lyophilized product. And they observed that in the case of a material on a nanometric scale, the NTA becomes interesting to quantify the material because it is more specific.

DLS and NTA detecting the hydrodynamic radii based on the equivalent sphere. Some authors have been discussing the theme, mainly the increase in the real size of the particles, presenting variations in the size of the samples that were executed in the same equipment (Little, Batchelor-Mcauley, Young & Compton, 2018; Niskanen et al., 2019).

Therefore, although the equipment is widely used in the field of nanotechnology, when dealing with non-spherical samples, it is not possible to point out the best option for checking the size of the particles. Arenas-Guerrero et al. (2018) were determined the size distribution of dispersed non-spherical nanoparticles. They were concluded that the use of commercial DLS provides a difficult estimation of the characteristic size of non-spherical particles, not a complete and accurate description of the sample.

3.1.6. Transmission electron microscopy (TEM)

The results of the transmission electron microscopy (TEM) analysis of the CNC are shown in Fig. 3.

The TEM did not support the analysis of the CNC. The hypothesis was that the sample had a high concentration of CNC and zeta potential around +15 mV; and it facilitated the agglomeration, which made it impossible to read the sample. Another hypothesis would be the delay in reading the sample, which may have facilitated the agglomeration of the CNC.

Our CNC TEM data were similar to Brandes, De Souza, Carminatti and Recouvreux (2020) who studied the production of CNC by enzymatic hydrolysis and observed that, in the TEM analysis, it is possible that cellulose hydrolysis promotes the breakdown of cellulose chains, especially in amorphous regions. And this can, at a given concentration, agglomerate the CNC.

3.2. Alginate particles and alginate particles covered by CNC

3.2.1. Surface zeta potential

Fig. 4 shows the results of the zeta potential on the surface of alginate particles without CNC, at different pH values.

The zeta potential of the CNC was positive (+15 mV). Therefore, for CNC adsorption on the surface of the particles, the alginate particle value must be negative. The results of the test indicated that the alginate particle zeta potential is negative and reaches the highest value of -26.46 ± 1.48 mV at pH 8.5, being chosen as the best condition to perform the alginate particle covering with the CNC due to the greater zeta potential value of the assay.
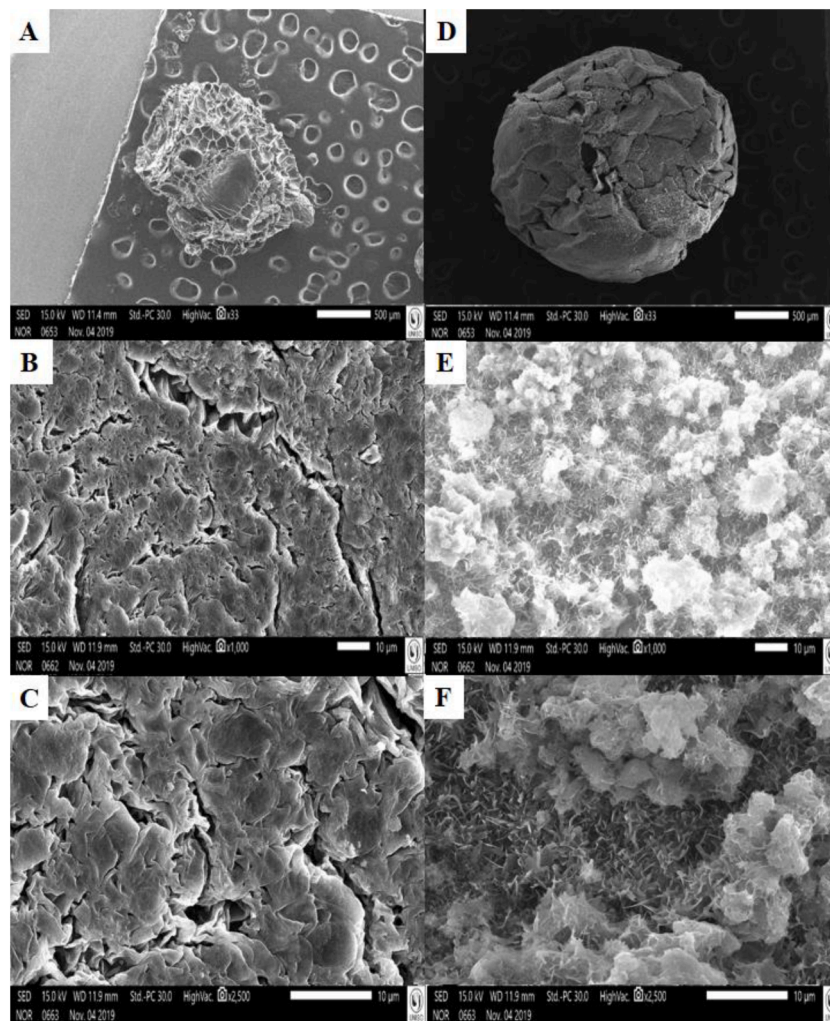
Fig. 8. Scanning electron microscopy (SEM) of alginate particles and alginate particles coated with CNC for 48 h. A, B, and C - Alginate particles with 33, 1000, and 2500x magnification. D, E, and F - Alginate particles + CNC with 33, 1000, and 2500x magnification.

When the our potential zeta results were compared to the Adebisi and Conway (2013) research, it was observed that both particles containing alginate are negative. In their paper, the results showed a zeta potential range of - 15.7 ± 1.7 mV and -9.8 ± 1.2 mV, and our particle showed a potential zeta of -26.46 ± 1.48 mV, indicating an increase in range because of the difference between the formulations.

3.2.2. Differential scanning calorimetry (DSC)

The DSC was performed to investigate the interaction of the compounds. The test results were presented by the thermograms of the alginate particles sample, alginate particles + CNC and CNC (Fig. 5).

The alginate particle thermogram reported the values at 64.65°C (endothermic peak) with 784.46 J/g (melting enthalpy). Two exothermic peaks were found at 308 and 378°C. A curve decay was identified. The CNC thermogram values were 62.65°C for the endothermic peak temperature and 128.07 J/g of melting enthalpy. A decay of the curve is observed and it is similar to the alginate particle sample.

The alginate particle+CNC sample thermogram proved to be more stable than the other samples. There was no presence of exothermic peaks; thus, characterizing the interaction between alginate and CNC. The temperature of the endothermic peak was 95.17°C with a melting enthalpy of 918.80 J/g.

In DSC tests, the two exothermic peaks that were found in alginate particle sample, are related to dehydration and depolymerization of alginate (Gohel & Patel, 2013; Sarmento, Ferreira, Veiga & Ribeiro,

2006). A curve decay that has been identified due to a change in calorific behavior is similar to the data of Martínez-gómez, Guerrero, Matsuhiro and Pavez (2017).

There are divergent values in the literature for alginate particles, mainly because of the difference between formulations. Peak values of 70.29 and 91.846°C were found, with an enthalpy of 181.3 and 211.49 J/g (Ahuja, Bhatia & Saini, 2016; Kassem et al., 2015).

There is no thermogram of CNC by enzymatic hydrolysis in the literature. However, the CNC data by acid hydrolysis for the endothermic peak is in the range of 140–195°C with enthalpy ranging from 51 to 95 J/g, indicating that the applied methodology interferes with the result of thermograms (Vasconcelos et al., 2017). A decay of the curve is observed in the research of George et al. (2011).

It is reported that when using CNC associated with polymers, the melting temperature, enthalpy, and crystalline behavior increase (George et al., 2011), as observed in our sample. This indicates that the CNC is adsorbed to the surface of the alginate particles, contributing to increase their stability.

3.2.3. Fourier transform infrared spectrometry (FTIR)

The spectrometry technique was used in order to compare the characteristic peaks of the samples and identify them according to the literature data. The results are presented through the spectra of the alginate particles samples, alginate particles + CNC and CNC (Fig. 6).

Concerning the sample referring to the alginate particles, peaks were

found on 524.16, 1080.14, 1627.52 cm^{-1}. The characteristic peaks found in the CNC sample were: 1627.52 and 3415.93 cm^{-1}. In the alginate particles + CNC sample, the peaks identified were: 524.16, 1080.14, 1627.52, 2359.04, 2921.6 and 3415.93 cm^{-1}. The peak 3415.93 cm^{-1} is similar to that found in the CNC sample. The peaks 524.16 and 1080.14 cm^{-1} were observed in the reference alginate particles samples. The 1624.52 cm^{-1} peak is present in both samples.

Nayak, Das and Maji (2012) described peaks at 3000–3600 cm^{-1} (stretching of -OH), 1614 cm^{-1} (-COO asymmetric), 1417 cm^{-1} -COO (symmetric), and 1032 cm^{-1} (C-O-C) about alginate particles. Vasconcelos et al. (2017) found data similar to ours in relation to FTIR CNC: 3362 cm^{-1} (OH elongation) and 1429 cm^{-1} (angular deformation CH).

This data showed the presence of characteristic groups of the standard samples (CNC and alginate particles) in the sample alginate particles + CNC and the coated was confirmed, proving the influence of the components in the analyzed sample.

3.2.4. Optical microscopy

The results are shown in Fig. 7. It is possible to observe that all alginate particles have a rounded shape but there is a difference between the standard sample and the sample with CNC in relation to the surface. The sample with CNC showed irregularity, while the other sample had a less rough surface.

Similar results of optical microscopy were presented in the paper of Ahuja et al. (2016) when performing the microscopy of the samples, describing them as spherical, but with an irregular shape and with rough surfaces, varying in size according to the sample formulation.

3.2.5. Scanning electron microscopy (SEM)

The data obtained in the test are shown in Fig. 8. In the microscopy images, in Figure A, it is possible to observe a change in the morphology of the alginate particles with CNC (figure D). When comparing figures B and E, the granules that are observed in E are not present in B. The larger granules are probably from the sucrose used in the lyophilization process. It is possible to identify the morphology of the CNC in figure F, proving that they adhere to the surface of the particles, demonstrating the effectiveness of the coating.

When comparing alginate particles to data from the literature, a similarity is observed in the images obtained by SEM, where uniform particles are identified (Santagapita, Mazzobre & Buera, 2012). Kalashnikova, Bizot, Bertoncini, Cathala and Capron (2013) analyzed a pickering emulsion stabilized with CNC by SEM. In the images, CNC was identified covering the extension of the drop, which is similar to our data.

4. Conclusions

The enzymatic hydrolysis is a green alternative for CNC production from bacterial cellulose. The mechanical treatment improved the production of the CNC, influencing the parameters of size, PDI, and zeta potential of the samples. When CNC was produced and applied in the alginate particles, a major stability in the system was observed, eliminating the agglomeration. The work results provide a new methodology for the CNC production by enzymatic hydrolysis and open a pathway to apply the CNC in alginate particles to improve the characteristics for pharmaceutical and food products. Moreover, the display showed a great pathway to the application of CNC, eliminating the technical problem, which is agglomeration. CNC can be applied to stabilize pickering emulsion; or in films and scaffolds as material for reinforcement. Also, this material will be a sustainable option for any company, with the possibility of increasing the shelf life of the products.

Declaration of Competing Interest

The authors declare no conflict of interest
The authors declare that they have no known competing financial interests or personal relationships that could have appeared to influence the work reported in this paper.

References

Abol-Fotouh, D., Hassan, M. A., Shokry, H., Roig, A., Azab, M. S., & Kashyout, A. E. H. B. (2020). Bacterial nanocellulose from agro-industrial wastes: Low-cost and enhanced production by Komagataeibacter saccharivorans MD1. *Scientific Reports, 10*(1), 3491. https://doi.org/10.1038/s41598-020-60315-9.

Adebisi, A. O., & Conway, B. R. (2013). Preparation and characterisation of gastroretentive alginate beads for. *Journal of Microencapsulation, 31*(1), 58–67. https://doi.org/10.3109/02652048.2013.805840.

Ahuja, M., Bhatia, M., & Saini, K. (2016). Sodium alginate – arabinoxylan composite microbeads : Preparation and characterization. *Journal of Pharmaceutical Investigation, 46*(7), 645–653. https://doi.org/10.1007/s40005-016-0244-1.

Alonso-Lerma, B., Barandiaran, L., Ugarte, L., Larraza, I., Reifs, A., Olmos-Juste, R., … Perez-Jimenez, R. (2020). High performance crystalline nanocellulose using an ancestral endoglucanase. *Communications Materials, 1*(1), 57. https://doi.org/10.1038/s43246-020-00055-5.

Alves, T. F. R., Barros, C. T., Baldo, D., Amaral, V. A., Sever, M., Santos, C., & Severino, P. (2018). Intestinal permeability studies of ibuprofen solid dispersion. *Journal of Dispersion Science and Technology, 40*(4), 546–554. https://doi.org/10.1080/01932691.2018.1472014.

Arenas-Guerrero, P., Delgado, Á. V., Donovan, K. J., Scott, K., Bellini, T., Mantegazza, F., & Jiménez, M. L. (2018). Determination of the size distribution of non-spherical nanoparticles by electric birefringence-based methods. *Scientific Reports, 8*(1), 9502. https://doi.org/10.1038/s41598-018-27840-0.

Arserim-uçar, D. K., Korel, F., Liu, L., & Yam, K. L. (2020). Characterization of bacterial cellulose nanocrystals: Effect of acid treatments and neutralization. *Food Chemistry.* , Article 127597. https://doi.org/10.1016/j.foodchem.2020.127597.

Bai, W., Holbery, Æ. J., & Li, Æ. K. (2009). A technique for production of nanocrystalline cellulose with a narrow size distribution. *Cellulose, 16*, 455–465. https://doi.org/10.1007/s10570-009-9277-1.

Benavides, S., Cortés, P., Parada, J., & Franco, W. (2016). Development of alginate microspheres containing thyme essential oil using ionic gelation. *Food Chemistry, 204*, 77–83. https://doi.org/10.1016/j.foodchem.2016.02.104.

Brandes, R., De Souza, L., Carminatti, C., & Recouvreux, D. (2020). Production with a high yield of bacterial cellulose nanocrystals by enzymatic hydrolysis. *International Journal of Nanoscience, 19*(3), 1–8. https://doi.org/10.1142/S0219581X19500157.

Chauve, G., Fraschini, C., & Jean, B. (2014). Separation of Cellulose Nanocrystals. *Handbook of green materials* (pp. 73–87). Grégory Chauve: Carole Fraschini and Bruno Jean. https://doi.org/10.1142/9789814566469_0006.

Choi, S. M., & Shin, E. J. (2020). The Nanofication and Functionalization of Bacterial Cellulose and Its Applications. *Nanomaterials, 10*(3), 406. https://doi.org/10.3390/nano10030406.

Criado, P., Fraschini, C., Jamshidian, M., Salmieri, S., Desjardins, N., Sahraoui, A., & Lacroix, M. (2019). Effect of cellulose nanocrystals on thyme essential oil release from alginate beads: Study of antimicrobial activity against Listeria innocua and ground meat shelf life in combination with gamma irradiation. *Cellulose, 26*(9), 5247–5265. https://doi.org/10.1007/s10570-019-02481-2.

Danaei, M., Dehghankhold, M., Ataei, S., Davarani, F. H., Javanmard, R., Dokhani, A., … Id, M. R. M. (2018). Impact of Particle Size and Polydispersity Index on the Clinical Applications of Lipidic Nanocarrier Systems. *Pharmaceutics, 10*(2), 57. https://doi.org/10.3390/pharmaceutics10020057.

de Souza, J. F., da Silva Pontes, K., Alves, T. F. R., Torqueti de Barros, C., Amaral, V. A., de Moura Crescencio, K. M., … Chaud, M. V. (2020). Structural comparison, physicochemical properties, and in vitro release profile of curcumin-loaded lyotropic liquid crystalline nanoparticle: Influence of hydrotrope as interface stabilizers. *Journal of Molecular Liquids, 306*, Article 112861. https://doi.org/10.1016/j.molliq.2020.112861.

Deepak, S. N., & Hari, B. N. V. (2013). Optimization, Development and evaluation of Microemulsion for the release of combination of Guaifenesin and Phenylephrine. *Journal of Applied Pharmaceutical Science, 3*(09), 48–56. https://doi.org/10.7324/JAPS.2013.3909.

Dugan, J. M., Gough, J. E., & Eichhorn, S. J. (2013). Bacterial cellulose scaffolds and cellulose nanowhiskers for tissue engineering. *Nanomedicine, 8*(2), 287–298. https://doi.org/10.2217/nnm.12.211.

Elazzouzi-hafraoui, s., Nishiyama, Y., Putaux, J., Heux, L., Dubreuil, F., & Rochas, C. (2008). The Shape and Size Distribution of Crystalline Nanoparticles Prepared by Acid Hydrolysis of Native Cellulose. *Biomacromolecules, 9*, 57–65.

George, J., Kumar, R., Sajeevkumar, V. A., Ramana, K. V., Rajamanickam, R., Abhishek, V., … Siddaramaiah. (2014). Hybrid HPMC nanocomposites containing bacterial cellulose nanocrystals and silver nanoparticles. *Carbohydrate Polymers, 105*(1), 285–292. https://doi.org/10.1016/j.carbpol.2014.01.057.

George, J., Ramana, K. V., Bawa, A. S., & Siddaramaiah. (2011). Bacterial cellulose nanocrystals exhibiting high thermal stability and their polymer nanocomposites. *International Journal of Biological Macromolecules, 48*(1), 50–57. https://doi.org/10.1016/j.ijbiomac.2010.09.013.

George, J., & Sabapathi, S. N. (2015). Cellulose nanocrystals: Synthesis, functional properties, and applications. *Nanotechnology, Science and Applications, 8*, 45–54. https://doi.org/10.2147/NSA.S64386.

Gohel, M. C., & Patel, T. M. (2013). Compatibility study of quetiapine fumarate with widely used sustained release excipients. *Journal of Thermal Analysis and Calorimetry, 111*(3), 2103–2108. https://doi.org/10.1007/s10973-012-2467-3.

Habibi, Y., Lucia, L. A., & Rojas, O. J. (2010). Cellulose nanocrystals: Chemistry, self-assembly, and applications. *Chemical Reviews, 110*(6), 3479–3500. https://doi.org/10.1021/cr900339w.

Jozala, A. F., Pértile, R. A. N., dos Santos, C. A., de Carvalho Santos-Ebinuma, V., Seckler, M. M., Gama, F. M., & Pessoa, A. (2014). Bacterial cellulose production by Gluconacetobacter xylinus by employing alternative culture media. *Applied Microbiology and Biotechnology, 99*(3), 1181–1190. https://doi.org/10.1007/s00253-014-6232-3.

Juárez-luna, G. N., Favela-torres, E., Quevedo, I. R., & Batina, N. (2019). Enzymatically assisted isolation of high-quality cellulose nanoparticles from water hyacinth stems. *Carbohydrate Polymers, 220*, 110–117. https://doi.org/10.1016/j.carbpol.2019.05.058 (May).

Kafle, K., Shin, H., Lee, C. M., Park, S., & Kim, S. H. (2015). Progressive structural changes of Avicel, bleached softwood, and bacterial cellulose during enzymatic hydrolysis. *Scientific Reports, 5*, 1–10. https://doi.org/10.1038/srep15102 (October).

Kalashnikova, I., Bizot, H., Bertoncini, P., Cathala, B., & Capron, I. (2013). Cellulosic nanorods of various aspect ratios for oil in water Pickering emulsions. *Soft Matter, 9*(3), 952–959. https://doi.org/10.1039/C2SM26472B.

Kale, S. N., & Deore, S. L. (2017). Emulsion micro emulsion and nano emulsion : A review. *Systematic Reviews in Pharmacy, 8*(1), 39–47.

Kassem, A. A., Farid, R. M., Issa, D. A. E., Abd-Allah, D. S. K., Abd-El-Razzak, M. Y., Saudi, H. I., … Arafa –Elzamarany, E. (2015). Development of mucoadhesive microbeads using thiolated sodium alginate for intrapocket delivery of resveratrol. *International Journal of Pharmaceutics, 487*(1–2), 305–313. https://doi.org/10.1016/j.ijpharm.2015.04.010.

Kim, J. H., Park, S., Kim, H., Kim, H. J., Yang, Y.-H., Kim, Y. H., … Lee, S. H. (2017). Alginate/bacterial cellulose nanocomposite beads prepared using Gluconacetobacter xylinus and their application in lipase immobilization. *Carbohydrate Polymers, 157*, 137–145. https://doi.org/10.1016/j.carbpol.2016.09.074.

Little, C. A., Batchelor-Mcauley, C., Young, N. P., & Compton, R. G. (2018). Shape and size of non-spherical silver nanoparticles: Implications for calculating nanoparticle number concentrations. *Nanoscale, 10*(34), 15943–15947. https://doi.org/10.1039/c8nr06062b.

Ma, M., Liu, Z., Hui, L., Shang, Z., Yuan, S., Dai, L., … Ni, Y. (2019). Lignin-containing cellulose nanocrystals/sodium alginate beads as highly effective adsorbents for cationic organic dyes. *International Journal of Biological Macromolecules, 139*, 640–646. https://doi.org/10.1016/j.ijbiomac.2019.08.022.

Martínez-gómez, F., Guerrero, J., Matsuhiro, B., & Pavez, J. (2017). In vitro release of metformin hydrochloride from sodium alginate /polyvinyl alcohol hydrogels. *Carbohydrate Polymers, 155*, 182–191. https://doi.org/10.1016/j.carbpol.2016.08.079.

Mohammed, N., Grishkewich, N., Berry, R. M., & Tam, K. C. (2015). Cellulose nanocrystal–alginate hydrogel beads as novel adsorbents for organic dyes in aqueous solutions. *Cellulose, 22*(6), 3725–3738. https://doi.org/10.1007/s10570-015-0747-3.

Morais, A. R.do V., Silva, A. L., Cojean, Sandrine Kaluvu Balaraman, C. B., Pomel, S., Barratt, G., … Loiseau, P. M. (2018). *In-vitro* and *in-vivo* antileishmanial activity of inexpensive amphotericin b formulations: Heated amphotericin B and amphotericin B-loaded microemulsion. *Experimental Parasitology, 192*, 85–92. https://doi.org/10.1016/j.exppara.2018.07.017.

Morais, J. P. S., Rosa, M. D. F., de Souza Filho, M., de sá, M., Nascimento, L. D., do Nascimento, D. M., & Cassales, A. R. (2013). Extraction and characterization of nanocellulose structures from raw cotton linter. *Carbohydrate Polymers, 91*(1), 229–235. https://doi.org/10.1016/j.carbpol.2012.08.010.

Morantes, D., Muñoz, E., Kam, D., & Shoseyov, O. (2019). Highly charged cellulose nanocrystals applied as a water treatment flocculant. *Nanomaterials, 9*(2), 272. https://doi.org/10.3390/nano9020272.

Nayak, A. K., Das, B., & Maji, R. (2012). Calcium alginate/gum arabic beads containing glibenclamide: Development and in vitro characterization. *International Journal of Biological Macromolecules, 51*(5), 1070–1078. https://doi.org/10.1016/j.ijbiomac.2012.08.021.

Ng, W. Y., Migotto, A., Ferreira, T. S., & Lopes, L. B. (2017). Monoolein-alginate beads as a platform to promote adenosine cutaneous localization and wound healing. *International Journal of Biological Macromolecules, 102*, 1104–1111. https://doi.org/10.1016/j.ijbiomac.2017.04.094.

Niskanen, I., Suopajärvi, T., Liimatainen, H., Fabritius, T., Heikkilä, R., & Thungström, G. (2019). Determining the complex refractive index of cellulose nanocrystals by combination of Beer-Lambert and immersion matching methods. *Journal of Quantitative Spectroscopy and Radiative Transfer, 235*, 1–6. https://doi.org/10.1016/j.jqsrt.2019.06.023.

Patel, M. A., AbouGhaly, M. H. H., Schryer-Praga, J. V., & Chadwick, K. (2017). The effect of ionotropic gelation residence time on alginate cross-linking and properties. *Carbohydrate Polymers, 155*, 362–371. https://doi.org/10.1016/j.carbpol.2016.08.095.

Patel, V. R., Dumancas, G. G., Viswanath, L. C. K., Maples, R., & Subong, B. J. J. (2016). Castor oil: Properties, uses, and optimization of processing parameters in commercial production. *Lipid Insights, 9*(1), 1–12. https://doi.org/10.4137/LPI.S40233.

Pereira, B., & Arantes, V. (2020). Production of cellulose nanocrystals integrated into a biochemical sugar platform process via enzymatic hydrolysis at high solid loading. *Industrial Crops and Products, 152*, Article 112377. https://doi.org/10.1016/j.indcrop.2020.112377 (December 2019).

Pirich, C. L., de Freitas, R. A., Torresi, R. M., Picheth, G. F., & Sierakowski, M. R. (2017). Piezoelectric immunochip coated with thin films of bacterial cellulose nanocrystals for dengue detection. *Biosensors and Bioelectronics, 92*, 47–53. https://doi.org/10.1016/j.bios.2017.01.068 (February).

Qiu, K., & Netravali, A. N. (2014). A review of fabrication and applications of bacterial cellulose based nanocomposites. *Polymer Reviews, 54*(4), 598–626. https://doi.org/10.1080/15583724.2014.896018.

Rovera, C., Fiori, F., Trabattoni, S., Romano, D., & Farris, S. (2020). Enzymatic hydrolysis of bacterial cellulose for the production of nanocrystals for the food packaging industry. *Nanomaterials, 10*(4), 1–11. https://doi.org/10.3390/nano10040735.

Rovera, C., Ghaani, M., Santo, N., Trabattoni, S., Olsson, R. T., & Farris, D. R. S. (2018). Enzymatic hydrolysis in the green production of bacterial cellulose nanocrystals. *ACS Sustainable Chemistry & Engineering, 6*(6), 7725–7734.

Santagapita, P. R., Mazzobre, M. F., & Buera, P. (2012). Invertase stability in alginate beads effect of trehalose and chitosan inclusion and of drying methods. *FRIN, 47*(2), 321–330. https://doi.org/10.1016/j.foodres.2011.07.042.

Sarmento, B., Ferreira, D., Veiga, F., & Ribeiro, A. (2006). Characterization of insulin-loaded alginate nanoparticles produced by ionotropic pre-gelation through DSC and FTIR studies. *Carbohydrate Polymers, 66*, 1–7. https://doi.org/10.1016/j.carbpol.2006.02.008.

Sousa, G. D., Kishishita, J., Aquino, K. A. S., Presgrave, O. A. F., Leal, L. B., & Santana, D. P. (2017). Biopharmaceutical assessment and irritation potential of microemulsions and conventional systems containing oil from syagrus cearensis for topical delivery of amphotericin B using alternative Methods. *AAPS PharmSciTech, 18*(5), 1833–1842. https://doi.org/10.1208/s12249-016-0663-3.

Vasconcelos, N. F., Feitosa, J. P. A., da Gama, F. M. P., Morais, J. P. S., Andrade, F. K., de Souza Filho, M.de S. M., & Rosal, M.de F. (2017). Bacterial cellulose nanocrystals produced under different hydrolysis conditions: Properties and morphological features. *Carbohydrate Polymers, 155*, 425–431. https://doi.org/10.1016/j.carbpol.2016.08.090.

Wang, J., Law, W. C., Chen, L., Chen, D., & Tang, C. Y. (2017). Fabrication of monodisperse drug-loaded poly(lactic-co-glycolic acid)–chitosan core-shell nanocomposites via pickering emulsion. *Composites Part B: Engineering, 121*, 99–107. https://doi.org/10.1016/j.compositesb.2017.03.032.

Yan, H., Chen, X., Song, H., Li, J., Feng, Y., Shi, Z., … Lin, Q. (2017). Synthesis of bacterial cellulose and bacterial cellulose nanocrystals for their applications in the stabilization of olive oil pickering emulsion. *Food Hydrocolloids, 72*, 127–135. https://doi.org/10.1016/j.foodhyd.2017.05.044.

Yan, H., Huang, D., Chen, X., Liu, H., Feng, Y., Zhao, Z., … Lin, Q. (2018). A novel and homogeneous scaffold material: Preparation and evaluation of alginate/bacterial cellulose nanocrystals/collagen composite hydrogel for tissue engineering. *Polymer Bulletin, 75*(3), 985–1000. https://doi.org/10.1007/s00289-017-2077-0.

Yi, T., Liu, C., Zhang, J., Wang, F., Wang, J., & Zhang, J. (2017). A new drug nanocrystal self-stabilized Pickering emulsion for oral delivery of silybin. *European Journal of Pharmaceutical Sciences, 96*, 420–427. https://doi.org/10.1016/j.ejps.2016.08.047.

You, J., Cao, J., Zhao, Y., Zhang, L., Zhou, J., & Chen, Y. (2016). Improved mechanical properties and sustained release behavior of cationic cellulose nanocrystals reinforeced cationic cellulose injectable hydrogels. *Biomacromolecules, 17*(9), 2839–2848. https://doi.org/10.1021/acs.biomac.6b00646.